Bijukchhen *et al. Earth, Planets and Space* (2017) 69:97
DOI 10.1186/s40623-017-0685-4

Earth, Planets and Space

FULL PAPER Open Access

Estimation of 1-D velocity models beneath strong-motion observation sites in the Kathmandu Valley using strong-motion records from moderate-sized earthquakes

Subeg M. Bijukchhen[1*], Nobuo Takai[2], Michiko Shigefuji[3], Masayoshi Ichiyanagi[4], Tsutomu Sasatani[5] and Yokito Sugimura[6]

Abstract

The Himalayan collision zone experiences many seismic activities with large earthquakes occurring at certain time intervals. The damming of the proto-Bagmati River as a result of rapid mountain-building processes created a lake in the Kathmandu Valley that eventually dried out, leaving thick unconsolidated lacustrine deposits. Previous studies have shown that the sediments are ~600 m thick in the center. A location in a seismically active region, and the possible amplification of seismic waves due to thick sediments, have made Kathmandu Valley seismically vulnerable. It has suffered devastation due to earthquakes several times in the past. The development of the Kathmandu Valley into the largest urban agglomerate in Nepal has exposed a large population to seismic hazards. This vulnerability was apparent during the Gorkha Earthquake (Mw7.8) on April 25, 2015, when the main shock and ensuing aftershocks claimed more than 1700 lives and nearly 13% of buildings inside the valley were completely damaged. Preparing safe and up-to-date building codes to reduce seismic risk requires a thorough study of ground motion amplification. Characterizing subsurface velocity structure is a step toward achieving that goal. We used the records from an array of strong-motion accelerometers installed by Hokkaido University and Tribhuvan University to construct 1-D velocity models of station sites by forward modeling of low-frequency *S*-waves. Filtered records (0.1–0.5 Hz) from one of the accelerometers installed at a rock site during a moderate-sized (mb4.9) earthquake on August 30, 2013, and three moderate-sized (Mw5.1, Mw5.1, and Mw5.5) aftershocks of the 2015 Gorkha Earthquake were used as input motion for modeling of low-frequency *S*-waves. We consulted available geological maps, cross-sections, and borehole data as the basis for initial models for the sediment sites. This study shows that the basin has an undulating topography and sediment sites have deposits of varying thicknesses, from 155 to 440 m. These models also show high velocity contrast at the bedrock depth which results in significant wave amplification.

Keywords: 1-D simulation, Velocity model, Propagator matrix, Diffused field theory, Kathmandu Valley

Introduction

The collision of the Eurasian and Indian tectonic plates forms an active plate boundary with many seismic events. The Nepal Himalaya regularly experiences small seismic activities, and large earthquakes occur over certain time intervals (Sapkota et al. 2013). The occurrence of strong ground motions in the Nepal Himalaya is comparatively less than other seismically active regions around the world. As a result of the collision, the Himalayan orogeny has formed a number of tectonic valleys in the region, including the Kathmandu Valley in the Nepal Himalaya. The formation and eventual drying of a lake has left the valley with thick (>600 m) unconsolidated sediments (Moribayashi and Maruo 1980; Sakai 2001).

The manifestation of an earthquake effect is a combination of source, path, and site characteristics. In addition

*Correspondence: subeg@eng.hokudai.ac.jp
[1] Graduate School of Engineering, Hokkaido University, Sapporo, Japan
Full list of author information is available at the end of the article

to the earthquake magnitude, site conditions play a vital role in the effect of earthquakes on infrastructure. An earthquake with seemingly no effect above hard ground can be felt as a strong tremor and cause severe damage in areas above soft or unconsolidated sediments due to the amplification of seismic waves. There are accounts of more than 20 devastating earthquakes occurring in or near the Nepal Himalaya after the thirteenth century (Dixit et al. 2013); the 2015 Gorkha Earthquake is the most recent. The Kathmandu Valley, along with a large part of central and eastern Nepal, suffered heavy loss of life and property due to the mainshock and ensuing aftershocks of the 2015 Gorkha Earthquake. According to Government of Nepal (2015), 8856 people lost their lives and more than 60,000 buildings were completely damaged. The Kathmandu Valley had 1739 casualties, and about 13% of buildings were estimated to have been completely damaged. A location in a seismically active region, and the presence of thick sediments that amplify seismic waves, have made the Kathmandu Valley a seismically vulnerable region. Moreover, the increasing tendency for haphazard building construction without proper engineering considerations has added to the potential for catastrophe.

A thorough study of ground motion amplification is required to prepare safe and up-to-date building codes that reduce loss of life and property during an earthquake. Characterizing subsurface velocity structures is a necessary precondition for achieving that goal. Previously, there was a study of 1-D velocity models in a few places in Kathmandu based on microtremors (Pandey 2000). A subsurface velocity model was prepared based on geological maps (Shrestha et al. 1998) and borehole logs collected during an earthquake disaster mitigation study (JICA 2002). Piya (2004) used available borehole data and geological information to prepare soil profiles of the valley sediment for liquefaction hazard analysis. The borehole logs available are predominantly from the groundwater wells in the Kathmandu Valley. The velocity logging below depths of 30 m is not publicly available. A study of basement structure using microtremor recordings from different locations in the valley, some of which lie in vicinity of the sites described in the present study, was carried out in 2012 (Paudyal et al. 2012).

In this study, we use seismic records of moderate earthquakes obtained from an array of strong-motion accelerometers (Fig. 1) to construct 1-D velocity models of the stations by forward modeling of low-frequency *S*-waves. A similar 1-D velocity model was prepared for seismic station KATNP, maintained by the United States Geological Survey (USGS), in Kathmandu using the mainshock of the Gorkha Earthquake (Dhakal et al. 2016). Furthermore, we examined our velocity models by comparing observed *H*-to-*V* spectral ratio with the theoretical *H*-to-*V* spectral ratio obtained from the models. Our ultimate goal is to prepare a 3-D subsurface model of the Kathmandu Valley using earthquake records; the present study is key piece of this objective.

Geological setting of the Kathmandu Valley

The Kathmandu Valley is a tectonic basin filled with fluvio-lacustrine deposits and surrounded by hills on all sides. The rapid uplift of the mountain range south of present-day Kathmandu dammed the proto-Bagmati River (Sakai et al. 2002) and formed the paleo-Kathmandu Lake (Fujii and Sakai 2002). The lake breached the hills and eventually dried out (at about 10 ka) leaving behind a sediment-filled valley (Sakai 2001). Since then, fluvial deposits from the Bagmati River system have overlain the older lake deposits. Previous studies (Moribayashi and Maruo 1980; Sakai 2001) have shown the sediments to be thicker than 600 m at the center of the valley. The hills surrounding the valley are formed of meta-sedimentary rocks with some granitic intrusions of Cambrian to Devonian origin (Stocklin and Bhattarai 1977). It is clear that the sediments in the valley are sourced from these basement rocks, as the lake in the past and the Bagmati River system at present are fed with water flowing from these very hills (Fig. 1). Figure 1 is based on the Engineering Geological Map of Kathmandu (1:50,000) published by Department of Mines and Geology (Shrestha et al. 1998).

The bottom and fringes of the valley have coarser sediments of the proto-Bagmati river system (Sakai 2001), which give way to finer sediments in the upper and central parts of the valley. The sedimentary layers in the valley can be generalized as coarser sand and gravel layers at the bottom superimposed with layers of sand and clay deposit of lacustrine facies; fluvial deposits from the Bagmati river system make up the topmost layer (Yoshida and Igarashi 1984; Dangol 1985; Shrestha et al. 1998; Sakai 2001). The sediment types in the valley generally vary from south to north, and the lithology has been differentiated into three main groups: southern, central, and northern (Sakai 2001; Piya 2004). The predominant sequence of thick black clay formed from a lacustrine environment in the southern and central region gives way to the sand-dominant sediments in the northern region. The clay layer diminishes in the north and pinches out to sandy/silty sediment (Sakai 2001) which has its origin in the granitic intrusion (Stocklin and Bhattarai 1977) in the northern surrounding hills.

Furthermore, borehole logs (Sakai 2001; JICA 2002; Piya 2004) have demonstrated a number of different layers and lenses formed due to varying depositional environments. The basin topography is highly undulated, and

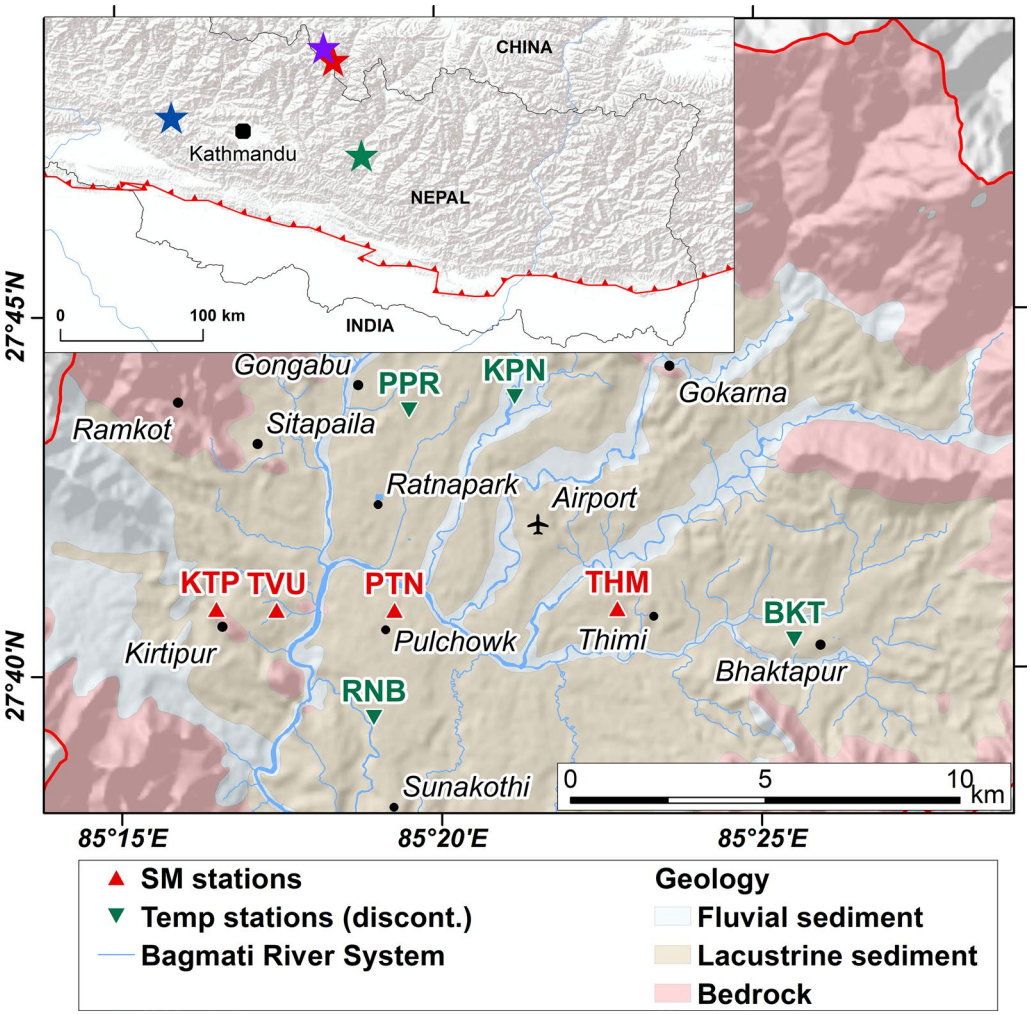

Fig. 1 Simplified geology of Kathmandu and location of strong-motion accelerometers. The temporary stations (*green triangles*) were added after the mainshock from the Gorkha Earthquake and were in operation for 3 months. *Inset* map of central and eastern Nepal showing the epicenters of the four earthquakes used in this study. The *red star* is the epicenter for the mb4.9 earthquake used to determine the 1-D models, the *purple star* is the epicenter for the Mw5.1 earthquake that occurred on April 25, 2015, 17:42 UTC, the *blue star* is the epicenter for the Mw5.1 that occurred at 23:16 UTC on the same day, and the *green star* is the epicenter for the Mw5.5 earthquake. The *red line* in the *inset* is the outline of the Himalayan Main Frontal Thrust

there are several rocky hillocks that breach through the thick sediments to the surface as bedrock exposures. One of these exposures can be seen in Kirtipur, where one of the accelerometers is installed (Fig. 1). The variation in basement topography, geology, and the depositional environment make it difficult to generalize the subsurface geologic structures and ground response of the valley as a whole. The lack of proper data on subsurface geology, velocity logs, and soil profiles makes the task challenging.

Strong-motion observation

A collaboration between Hokkaido University, Japan, and Central Department of Geology (CDG), Tribhuvan University, Nepal, began in 2011 to study the strong-motion characteristics in Kathmandu Valley (Takai et al. 2016). Four strong-motion accelerometers (Mitsutoyo JEP-6A3-2) were installed at KTP, TVU, PTN, and THM, in a west to east array (Fig. 1). These accelerometers are bolted to the ground floor of reinforced concrete (RC) buildings, except at PTN where the building is a single story masonry structure. These accelerometers operate continuously at a sampling rate of 100 Hz, and the time calibration is carried out using GPS. Although the data loggers are powered with regular 200 V AC supply, backup batteries are employed due to inconsistent electricity supply in the valley. The seismometers recorded a

number of earthquakes including the Gorkha Earthquake on April 25, 2015, and its subsequent aftershocks. The seismic activity has largely increased after the Gorkha Earthquake. Four more temporary stations (BKT, RBN, PPR, and KPN) were deployed for 3 months (May 8 to August 6, 2015), after the Gorkha Earthquake, to observe aftershock activity.

The station KTP lies in Kirtipur, west Kathmandu, on a rock site. The stations TVU (CDG, Tribhuvan University), PTN (Pulchwok Campus, Patan), and THM (University Grants Commission, Sano-Thimi) are the sediment sites (Fig. 1). The shear wave velocity (V_s) of the shallow subsurface layer measured during their installation shows V_s ~700 m/s at KTP and ~200 m/s at other sites (Takai et al. 2015). The absence of prominent peaks in the average H/V ratio of microtremors at KTP and early arrival of S-waves at KTP compared to other sites during earthquakes (Bijukchhen et al. 2015) indicate that KTP is a rock site; there is likely a weathered and fractured layer of exposed bedrocks overlying the basement rocks at depth. The temporary stations, BKT (Bhaktapur), RNB (Ranibu), PPR (Panipokhari), and KPN (Kapan), were installed more or less normal to the existing W–E profile (Fig. 1). All four were installed over the sediment sites.

The sedimentary sites show high amplification of seismic waves. This can be observed from the moderate earthquake (mb4.9) that occurred about 80 km NE of Kathmandu (Fig. 1) near the Tibetan border on August 30, 2013. The Fourier spectra of the transverse component of the earthquake (Fig. 2) demonstrate the presence of low-frequency waves and their large amplification at the sedimentary sites compared to that at KTP. The spectral ratio, i.e., the ratio of the Fourier spectrum of the sedimentary site to that of the rock site, confirms this hypothesis.

We selected three more moderate earthquakes, all aftershocks of the Gorkha Earthquake, to study. Two of them, both Mw5.1, occurred on the same day as the mainshock (April 25, 2015). The first one occurred at 17:42 UTC with an epicenter ~80 km northeast of Kathmandu (Fig. 3). The other one had an epicenter about 45 km west of Kathmandu and occurred at 23:16 UTC (Fig. 4). The four temporary sites were added a week after the mainshock, so they lack records of all three earthquakes. Therefore, we considered an additional earthquake (Mw5.5) that occurred on May 16, 2015, about 75 km east of Kathmandu, which was recorded at all eight stations (Figs. 5, 6).

The forms of the Fourier spectra of the rock site (KTP) depend on f^2 for low frequencies ($f < 1$ Hz) except for the Mw5.5 event. This spectral form resulted from incidence of the low-frequency S-wave beneath the KTP site. The higher frequencies ($f > 1$ Hz) do not depend on f^0 effect

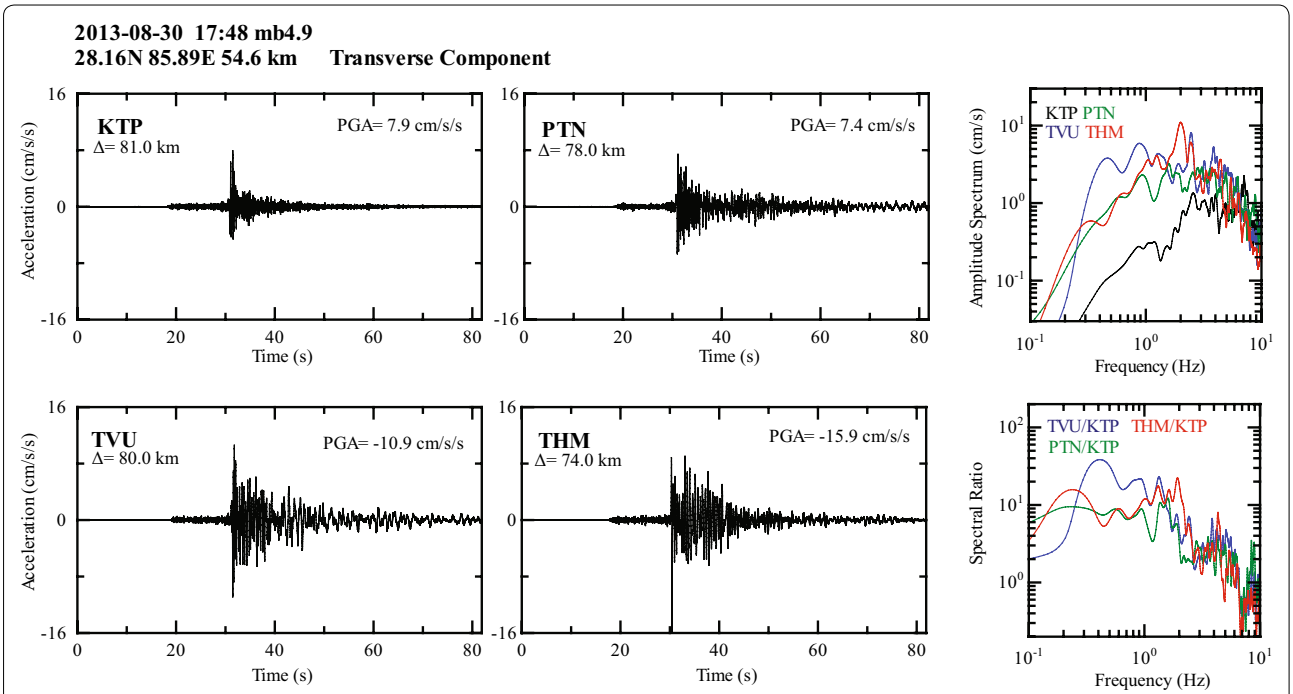

Fig. 2 Acceleration waveforms, Fourier spectra, and spectral ratios of the mb4.9 earthquake for the transverse component. The epicenter of the earthquake is about 80 km NE of Kathmandu. The record of this earthquake was used to adjust the initial 1-D velocity model. A significant amplification in the low-frequency region is clearly evident

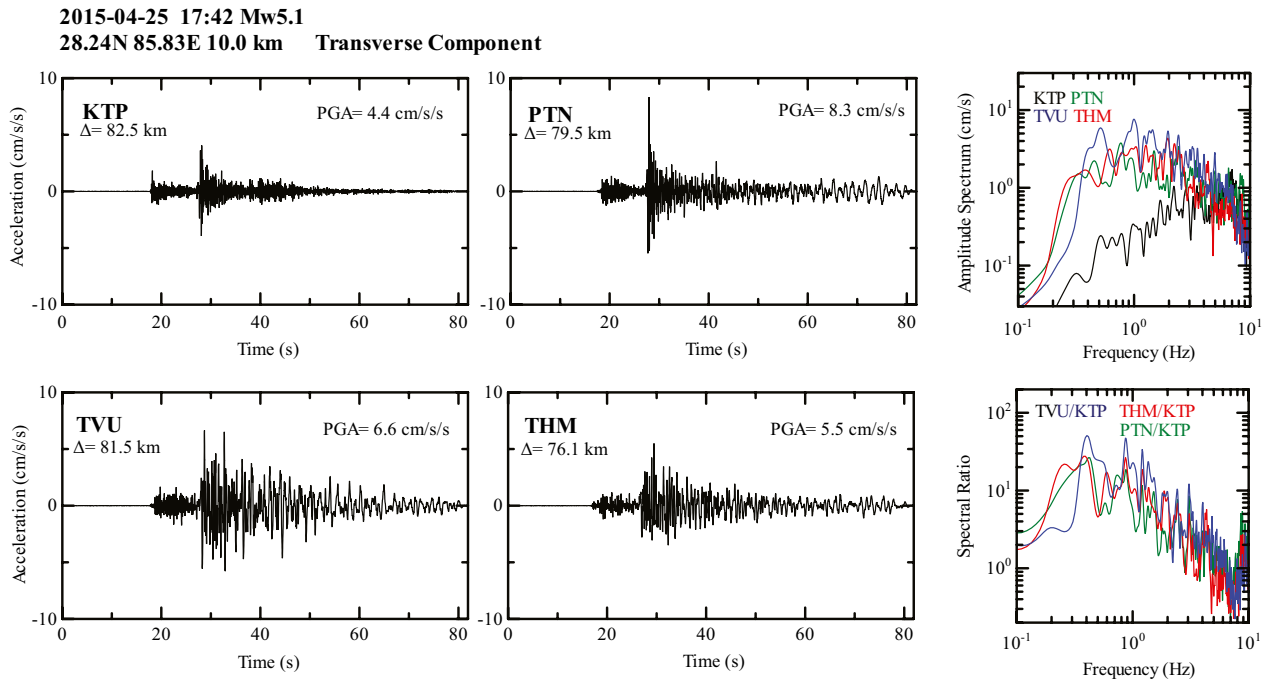

Fig. 3 Acceleration waveforms, Fourier spectra, and spectral ratios of the Mw5.1 earthquake for the transverse component. This aftershock (April 25, 2015 17:42 UTC) occurred NE of Kathmandu, near the epicenter of the mb4.9 earthquake

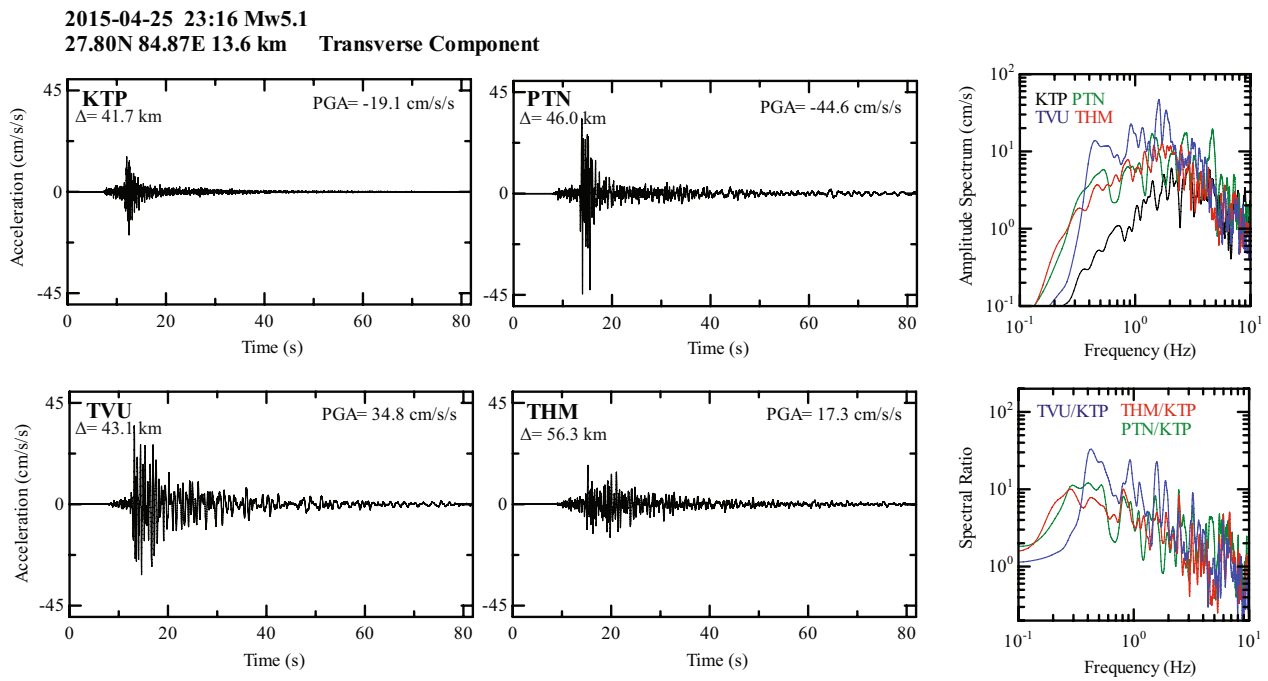

Fig. 4 Acceleration waveforms, Fourier spectra, and spectral ratios of the second Mw5.1 earthquake for the transverse component. The epicenter of this aftershock (April 25, 2015 23:16 UTC) is about 45 km west of Kathmandu

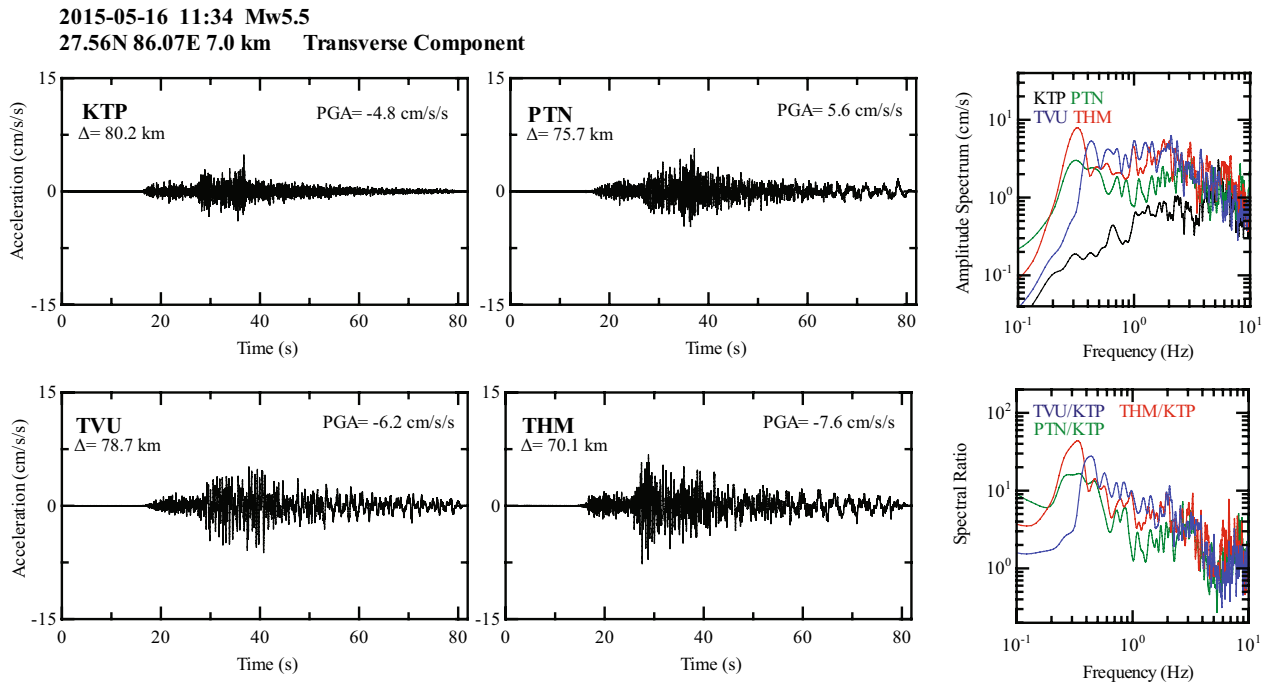

Fig. 5 Acceleration waveforms, Fourier spectra, and spectral ratios of the Mw5.5 aftershock for the transverse component. This aftershock occurred on the same day as the largest aftershock (Mw7.3) about 75 km east of Kathmandu

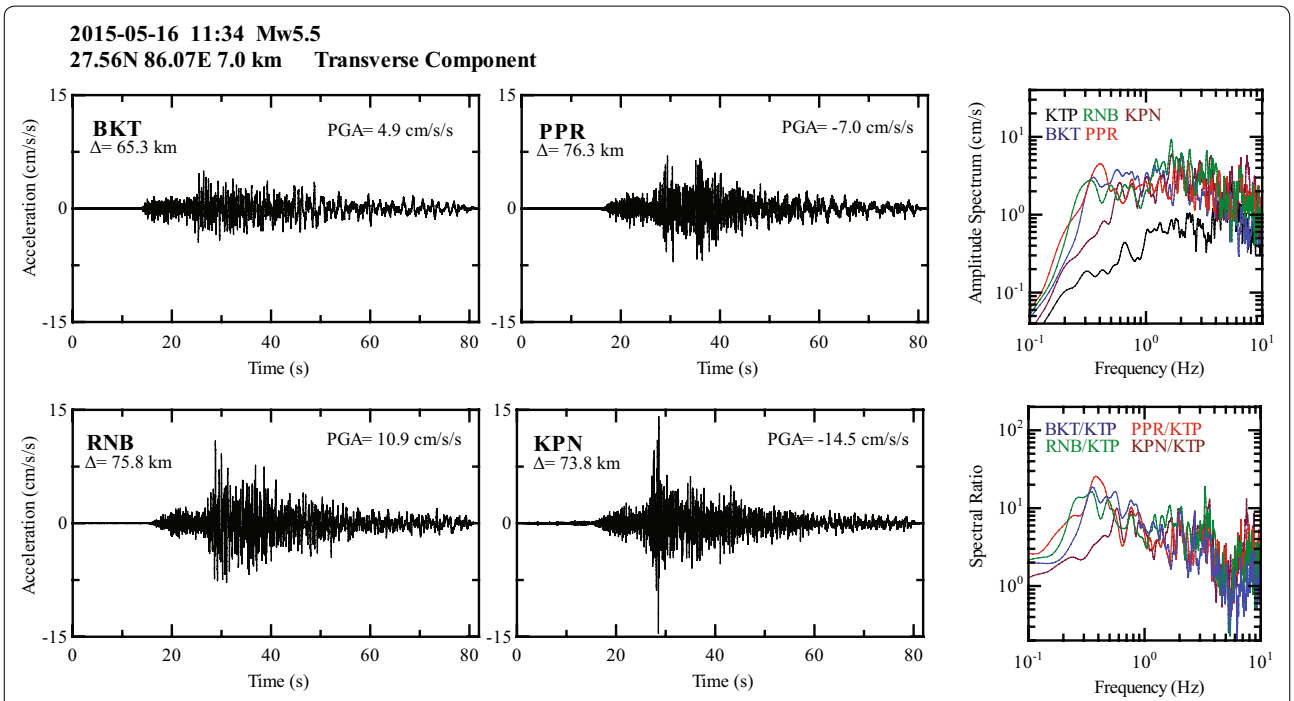

Fig. 6 Acceleration waveforms, Fourier spectra, and spectral ratios of the Mw5.5 aftershock for the transverse component. This aftershock occurred on the same day as the largest aftershock (Mw7.3)

of a weathered rock layer at the top. The spectra of the sedimentary sites show larger amplitudes in $0.2 < f < 2$ Hz than those at KTP. There is sharp increase in amplitude at low frequencies between 0.2 and 0.4 Hz at the sedimentary sites for all earthquakes. It should be noted that as the window length for the spectral analysis in Figs. 2, 3, 4, 5 and 6 is 80 s, and the high amplitude observed is pertinent to *S*-wave amplification as well as excitation of basin-induced surface waves.

Methodology

The response of a laterally heterogeneous sedimentary basin to incident *S*-waves is to produce *S*-wave amplification and basin-induced surface waves. The direct long-period *S*-wave from a 3-D simulation for a deep basin structure is essentially same as that from 1-D simulation for a flat-layered structure beneath the site (Dhakal et al. 2009, 2011). As an initial step in the 3-D simulation of Kathmandu Valley basin, a 1-D velocity structure estimation was conducted using forward modeling of an observed long-period *S*-wave from the mb4.9 earthquake. We used the Propagator Matrix method (Aki and Richards 2000) which relates the incident wave to its surface displacement, in 1-D simulation of the theoretical long-period *S*-wave. When a waveform incident at angle j propagates through a layer with density ρ, the motion stress vector $\boldsymbol{f}(z)$ at depth z can be related to the motion stress vector at the surface $\boldsymbol{f}(z_0)$ with a matrix $\mathbf{P}$, known as the Propagator Matrix.

$$\boldsymbol{f}(z) = \boldsymbol{P}(z, z_0)\boldsymbol{f}(z_0) \tag{1}$$

For the horizontal component of *S*-wave, the Propagator Matrix for a layer is

$$\boldsymbol{P}(z, z_0) = \begin{bmatrix} \cos[\omega\eta(z - z_0)] & (\omega\mu\eta)^{-1}\sin[\omega\eta(z - z_0)] \\ -(\omega\mu\eta)\sin[\omega\eta(z - z_0)] & \cos[\omega\eta(z - z_0)] \end{bmatrix} \tag{2}$$

where $\eta = \frac{\cos j}{V_s}$ and $\mu = \rho V_s^2$.

For n layers above a half space, Eq. (1) becomes.

$$\boldsymbol{f}(z_n) = \boldsymbol{P}(z_n, z_{n-1})\boldsymbol{P}(z_{n-1}, z_{n-2}) \ldots \boldsymbol{P}(z_1, z_0)\boldsymbol{f}(z_0)$$

$$\boldsymbol{f}(z_n) = \widehat{\boldsymbol{P}}(z_n, z_0)\boldsymbol{f}(z_0) \tag{3}$$

The motion stress vector $\boldsymbol{f}(z)$ can be written in terms of amount of down-going wave $\grave{S}$ and amount of up-going wave $\acute{S}$ as

$$\boldsymbol{f}(z_n) = \boldsymbol{F}(z_n)\begin{pmatrix} \grave{S} \\ \acute{S} \end{pmatrix} \tag{4}$$

From Eqs. (3) and (4), we obtain

$$\begin{pmatrix} \grave{S} \\ \acute{S} \end{pmatrix} = \boldsymbol{E}^{-1}(z_n)\widehat{\boldsymbol{P}}(z_n, z_0)\begin{pmatrix} l_0 \\ 0 \end{pmatrix}_{z=z_0} \tag{5}$$

where $\boldsymbol{E}^{-1}(z_n)$ is defined as

$$\boldsymbol{E}^{-1}(z_n) = \begin{bmatrix} \frac{1}{2} & \frac{-i}{2\omega\mu\eta} \\ \frac{1}{2} & \frac{i}{2\omega\mu\eta} \end{bmatrix}$$

From Eq. (5), we obtain

$$\begin{pmatrix} \grave{S} \\ \acute{S} \end{pmatrix} = \boldsymbol{B}(z_n, z_0)\begin{pmatrix} l_0 \\ 0 \end{pmatrix} \tag{6}$$

When the incident wave is known, its surface displacement l_0, after passing through n layers, can be estimated with

$$l_0 = \frac{\acute{S}}{\boldsymbol{B}_{21}} \tag{7}$$

The long-period (0.1–0.5 Hz) transverse component of the acceleration waveform from the rock site (KTP) during the mb4.9 earthquake was considered as the incident wave, and simulated waveforms from the three sediment sites were calculated using Eq. (7). Although the bedrock at KTP is overlain with a shallow weathered rock layer, this material has little or no effect on the long-period waves we are using in this study. As this earthquake originated at >50 km depth, we assumed that the seismic waves impinged on the bedrock beneath the basin perpendicularly. The information regarding damping of soil layers in Kathmandu Valley is not available, so we fixed $Q = 0.1\ V_s$ (V_s in m/s) which is commonly used for long-period strong-motion simulation (Olsen et al. 2000; Satoh 2004).

Available borehole data (Sakai et al. 2001; JICA 2002; Piya 2004), a geological map (Shrestha et al. 1998), and geological cross-sections were synthesized to create the initial subsurface models. The shear wave velocity was based on the earthquake disaster mitigation report (JICA 2002), and the number of layers was based on the geological cross-sections. The shear wave velocity of bedrock was fixed as 3.2 km/s from a regional velocity model of the Himalaya (Monsalve et al. 2006; Ichiyanagi et al. 2016). We used a pulse of the band-pass-filtered (0.1–0.5 Hz) acceleration waveform from KTP as input motion passing through the initial models and obtained simulated ground motions at the sediment sites. The bandwidths were chosen considering the spectral ratio in the low-frequency range in all the earthquake records. The thicknesses of the layers were then adjusted using trial and error to match the simulated waveforms with observed ones. These adjusted 1-D velocity models were then used to simulate the long-period *S*-waves of the three aftershocks, two Mw5.1 and a single Mw5.5, after the Gorkha Earthquake. These simulated *S*-waves were compared with the observed ones to verify the adjusted models.

We used band-pass-filtered transverse components of the aftershock records at KTP as the input motions. Because these earthquakes have shallow hypocenters, the incident angle was considered to be 30°, based on trial and error.

As a method of verifying the velocity models estimated by modeling long-period *S*-waves using the Propagator Matrix method, we employed the *H*-to-*V* spectral ratio (HVSR) method. It uses the horizontal-to-vertical spectral ratio of observed earthquakes for inversion of layered structures based on the diffused field theory for plane body waves (Kawase et al. 2011; Nagashima et al. 2014). The following equation relates the H/V ratio of plane body waves to transfer functions of horizontal motion and vertical motion on the surface due to vertically incident *S*-wave and *P*-wave, respectively:

$$\frac{H(\omega)}{V(\omega)} = \sqrt{\frac{\alpha_H}{\beta_H}} \frac{|TF_1(\omega)|}{|TF_3(\omega)|} \tag{8}$$

where α_H and β_H are, respectively, the *P*-wave and *S*-wave velocities of bedrock, TF_1 is the transfer function for horizontal motion on the surface due to a vertically incident *S*-wave at bedrock, and TF_3 is transfer function for vertical motion on the surface due to a vertically incident *P*-wave.

We used Eq. (8) to estimate the theoretical H/V ratio using the adjusted velocity models. The value of Q was set to 0.1 V_s for this method as well. The *P*-wave velocities of the layers were estimated as a function of shear wave velocity based on previous studies in the Himalayan region: $V_p/V_s = 1.73$ for basement rocks (Monsalve et al. 2006) and $V_p/V_s = 2.5$ for sedimentary layers (Borah et al. 2015). We selected 10 moderate aftershocks (M5–M5.5) of the Gorkha Earthquake (Table 1) and compared their observed average H/V ratios with the theoretical H/V ratios calculated using Eq. (8).

Table 1 Moderate earthquakes considered for the HVSR method for fixed stations. The magnitudes of the earthquakes range from M5 to M5.5

S no.	Date	Lat long	Dep (km)	Magnitude
1	2015-04-25 06:37	27.744N 85.830E	10.0	mb5.1
2	2015-04-25 06:56	27.882N 85.751E	10.0	mb5.5
3	2015-04-25 12:44	28.098N 84.559E	10.0	mb5.2
4	2015-04-25 17:42	28.238N 85.829E	10.0	Mw5.1
5	2015-04-25 23:16	27.799N 84.871E	13.6	Mw5.1
6	2015-05-12 07:17	27.714N 86.218E	13.0	mb5.5
7	2015-05-12 07:34	27.746N 86.245E	10.0	mb5.4
8	2015-05-12 08:21	27.730N 86.132E	15.0	mb5.2
9	2015-05-12 21:25	27.783N 86.638E	10.0	mb5.2
10	2015-05-16 11:34	27.560N 86.073E	7.0	Mw5.5

The HVSR method has been used to generate a 1-D velocity structure in Tohoku, Japan (Nagashima et al. 2014), confirming that the method could be employed to estimate the 1-D structure at our study sites. The temporary stations added after the main shock do not have records of the m4.9 earthquake, so we employed the HVSR method for the 1-D velocity model estimation.

We prepared the initial 1-D velocity models using the geological cross-sections, as we did for the permanent stations, and then used the HVSR method to adjust them. For the process, we considered the observed average H/V ratios from eight moderate (M5–M5.5) aftershocks (Table 2) and compared them with the theoretical H/V ratios for the velocity models using trial and error. The adjusted models were then used to simulate the theoretical long-period *S*-waves from the aftershock (Mw5.5) of the Gorkha Earthquake applying the Propagator Matrix method for all seven sites.

Despite the availability of a number of aftershock records, many were small and low energy in the long-period range, so they were not considered in this study. Moreover, a number of moderate-sized aftershocks in our database were affected by continuous smaller aftershocks occurring for a few seconds. The quality of the records was a constraint in choosing the earthquake for the modeling of the observed long-period *S*-wave. However, for larger earthquakes, because they are affected by the nonlinear site response of valley sediment (Dhakal et al. 2016; Rajaure et al. 2016), the nonlinear response needs to be taken into account when used for similar calculations.

Results

The velocity models were adjusted by trying to match the simulated long-period *S*-wave with the observed records from the mb4.9 earthquake (Fig. 7). Our calculations using the adjusted velocity models (Fig. 8), estimated by modeling the long-period *S*-wave, returned simulated

Table 2 Earthquakes considered for the HVSR method for four temporary stations

S no.	Date	Lat long	Dep (km)	Magnitude
1	2015-05-12 07:17	27.714N 86.218E	13.00	mb5.5
2	2015-05-12 07:34	27.746N 86.245E	10.00	mb5.4
3	2015-05-12 08:06	27.722N 86.061E	15.00	mb5
4	2015-05-12 08:13	27.760N 86.760E	15.00	mb5.1
5	2015-05-12 08:21	27.730N 86.132E	15.00	mb5.2
6	2015-05-12 21:25	27.783N 86.638E	10.00	mb5.2
7	2015-05-13 21:38	27.720N 86.050E	8.40	mb5
8	2015-05-16 11:34	27.560N 86.073E	7.00	Mw5.5

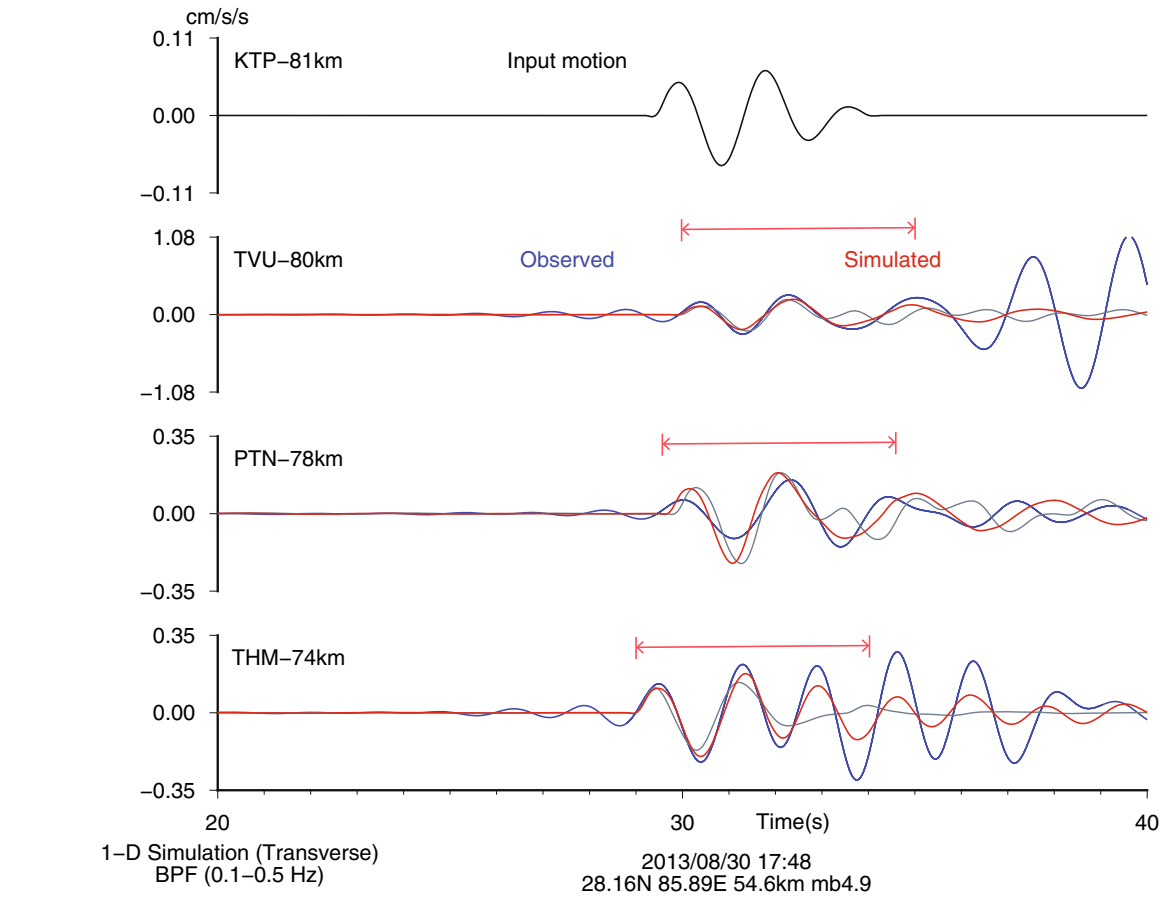

Fig. 7 Comparison between simulated and observed waveforms for the mb4.9 earthquake. Also shown is the result using the initial model, in *gray*. Waveform matching was conducted using trial and error for time windows indicated by the *red arrows*

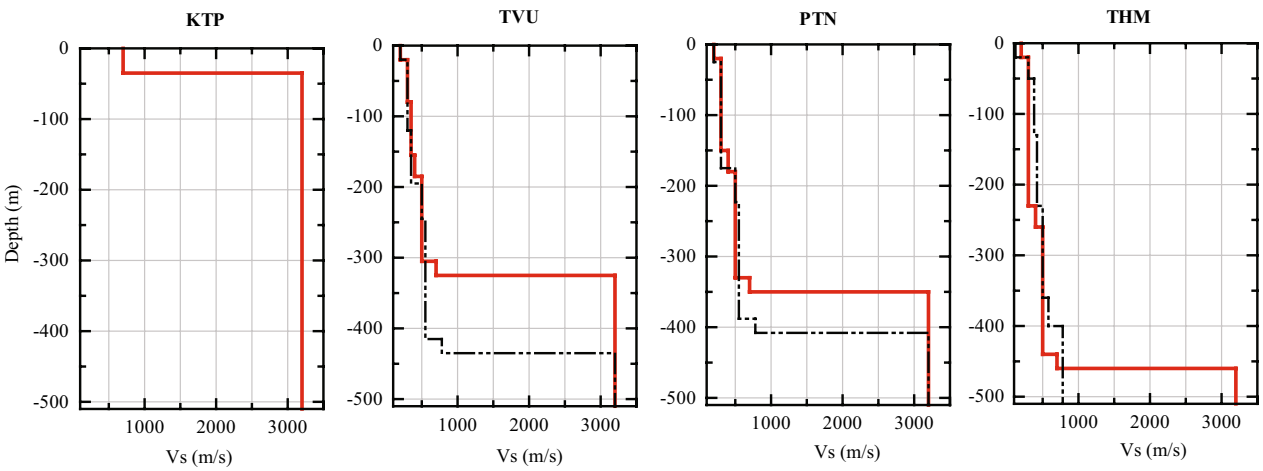

Fig. 8 1-D velocity models for four fixed sites. The model for KTP was considered as a bedrock site overlain by a layer of weathered rock and those for TVU, PTN, and THM are adjusted 1-D velocity models. Site THM has the *thickest sediment*. The *black dashed lines* indicate the initial velocity model prepared based on geological maps, cross-sections, and available borehole data

waveforms with good agreement to the observed ones from the earthquakes. The simulated *S*-waves using the adjusted velocity models for both Mw5.1 aftershocks (Figs. 9, 10) had good fits at PTN, whereas at TVU and THM, there are discrepancies in the amplitude. In contrast, the simulated *S*-waves for the Mw5.5 earthquake (Fig. 11) were better agreement at THM and PTN. These figures also show the difference between the simulation results using the initial velocity models and adjusted models. These observed waveforms have larger amplitudes compared with the simulated ones in the later phases, as the complex basement topography and 3-D basin topography might have played a role in their amplification, which cannot be simulated properly with only 1-D structures.

The comparison of the average H/V ratios from observed records and the theoretical H/V ratios (the HVSR method) shows agreement in the low-frequency (long-period) range (Fig. 12). The fundamental peaks of the H/V ratios range from 0.25 to 0.4 Hz for the sedimentary sites. The figure also shows the difference between results from the initial velocity model and adjusted velocity model. The fundamental frequencies of the observed and theoretical H/V ratio (the HVSR method) at TVU show considerably better agreement than those at the other sites. However, there are discrepancies in the high-frequency range, suggesting that velocity models need adjustments at higher frequencies. Both the H/V ratios at KTP are similar in shape, a flat profile with no clear peak, in the low-frequency range (<1 Hz), while they are not similar in shape in the high-frequency range (>1 Hz). This suggests that we need to adjust the KTP velocity model.

The 1-D velocity models for the four temporary sites (Fig. 13) were adjusted using the HVSR method. Similar to the four fixed stations, the fundamental frequency and amplitude in the lower frequency range show better agreement (Fig. 14) with the observed H/V ratio. The

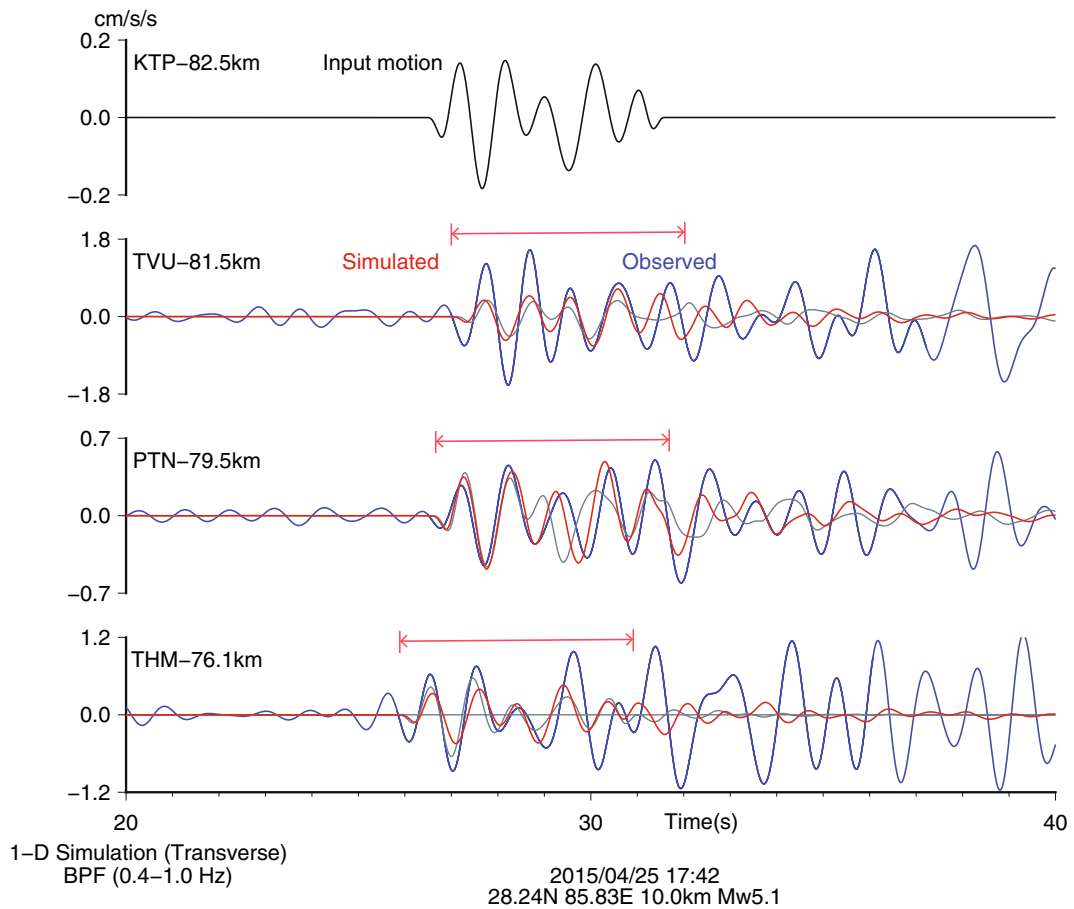

Fig. 9 Simulation of the Mw5.1 earthquake using the adjusted velocity model. The observed amplification at TVU is larger than the simulated waveform. The *gray* waveform is the result from the Propagator Matrix method using the initial velocity model. Waveform matching was conducted using trial and error for time windows indicated by the *red arrows*

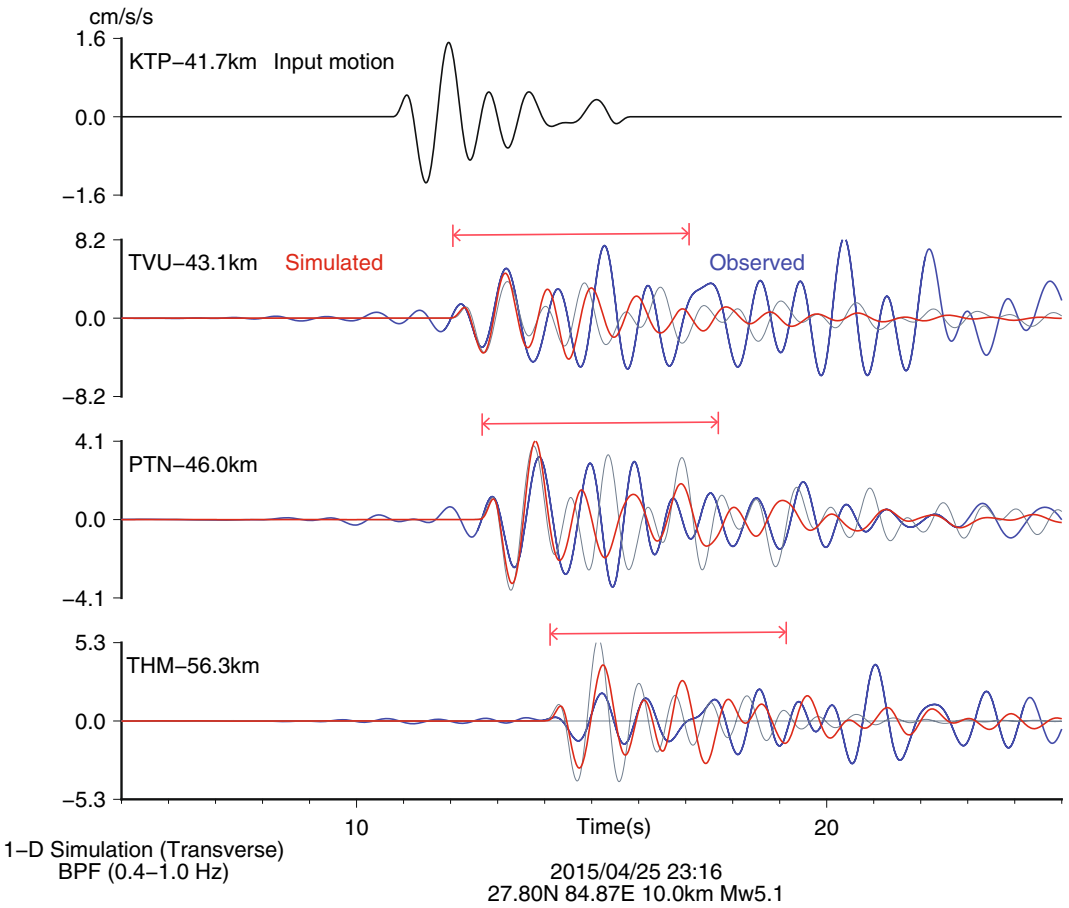

Fig. 10 Simulation of the second Mw5.1 earthquake. The simulated waveforms at TVU and PTN have similar amplitudes with the observed waveform; however, at THM, the simulation is overestimated. The result from the initial model is also shown, in *gray*. Waveform matching was conducted using trial and error for time windows indicated by the *red arrows*

fundamental frequencies for the sites range from 0.3 to 0.7 Hz. Better tuning at higher frequencies is required; this is the next phase of our study. The simulated waveform for the Mw5.5 earthquake using the 1-D velocity model provided encouraging results (Fig. 15). The simulated and observed waveforms for sites RNB and KPN show better agreement in both frequency and amplitude. However, the BKT site needs finer tuning; the presence of a pond near the BKT site might have some effect on the observed waveform. In general, we found that we can use the HVSR method to determine the subsurface structure of the Kathmandu Valley.

The 1-D velocity models (Figs. 8, 13) of the sediment show varying sediment thicknesses (bedrock depths) for the sites in the Kathmandu Valley. The depth of bedrock varies from 155 m at KPN to 440 m at THM. Because THM is not in the central part of the basin, the depth might increase at the center. As indicated previously, the dominant clay layer in the central valley transitions to a sandy layer in the north; this observation has been taken into account while adjusting the velocity models for the northern sites, PPR and KPN (Fig. 13). As we consulted and based our initial models on the geological cross-sections and borehole logs near the PPR site (JICA 2002), which showed the dominance of sandy layer with lenses of clay layers, the adjusted models (Fig. 13) show a velocity inversion at PPR. Another feature of the velocity models (Figs. 8, 13) is a large velocity contrast at the bedrock depth. This is due to a geological unconformity in the lithological sequence, where soft sediments of the proto-Bagmati lake deposited over the layer of weathered basement rocks during the valley formation.

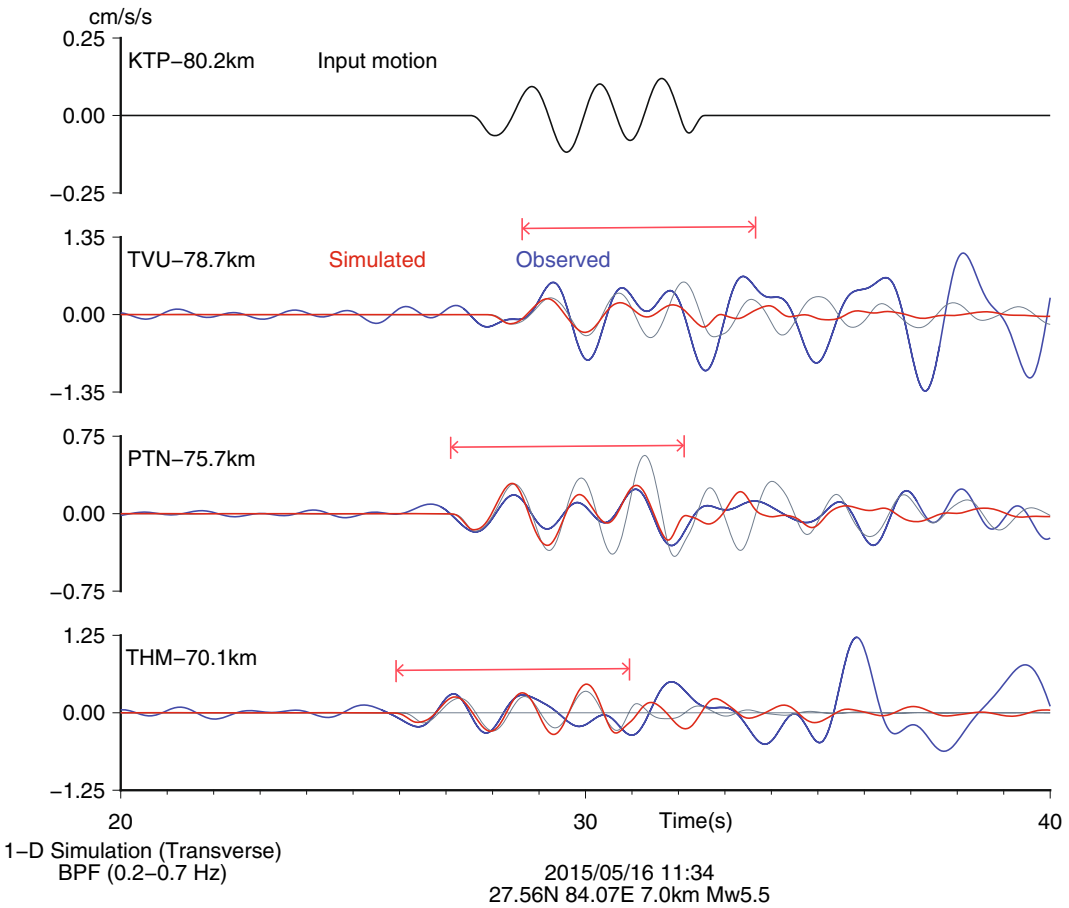

Fig. 11 Comparison of observed and simulated waveforms for the Mw5.5 earthquake. The observed waveform at TVU has a higher amplification than the simulated waveforms. A comparison of results from the initial model (*gray*) and adjusted model (*red*) show that a better agreement is obtained when using the adjusted model. Waveform matching was conducted using trial and error for time windows indicated by the *red arrows*

A previous study using 1-D modeling near the central Kathmandu showed that sediment depth was ~450 m (Pandey 2000; Dhakal et al. 2016). The depth of basement rock calculated using an empirical relationship with the fundamental frequency of ambient seismic noise (Paudyal et al. 2013) indicated that the valley center is 347 m deep. While some of the ambient noise measurement sites from Paudyal et al. (2013) lie in the vicinity of our stations, the previously calculated sediment thicknesses are less than those calculated in the present study. Our study estimates sediment thickness beneath TVU as 325 m, and the ambient noise study indicated a thickness of 65–138 m beneath two nearby sites. Nevertheless, it clearly shows that the valley basin has an undulating topography. The theoretical amplification obtained from the Propagator Matrix method (Fig. 16) shows the variation between the sites in the form of a difference in fundamental frequency. The amplification also indicates uneven basement topography, which makes generalizing the effects of earthquakes difficult.

Conclusions

We estimated 1-D velocity models for seven sites in the Kathmandu Valley using strong-motion records from moderate-sized earthquakes. First, the initial 1-D velocity models were constructed based on available geological data, borehole logs, and cross-sections. Second, we adjusted velocity models from the initial models, by

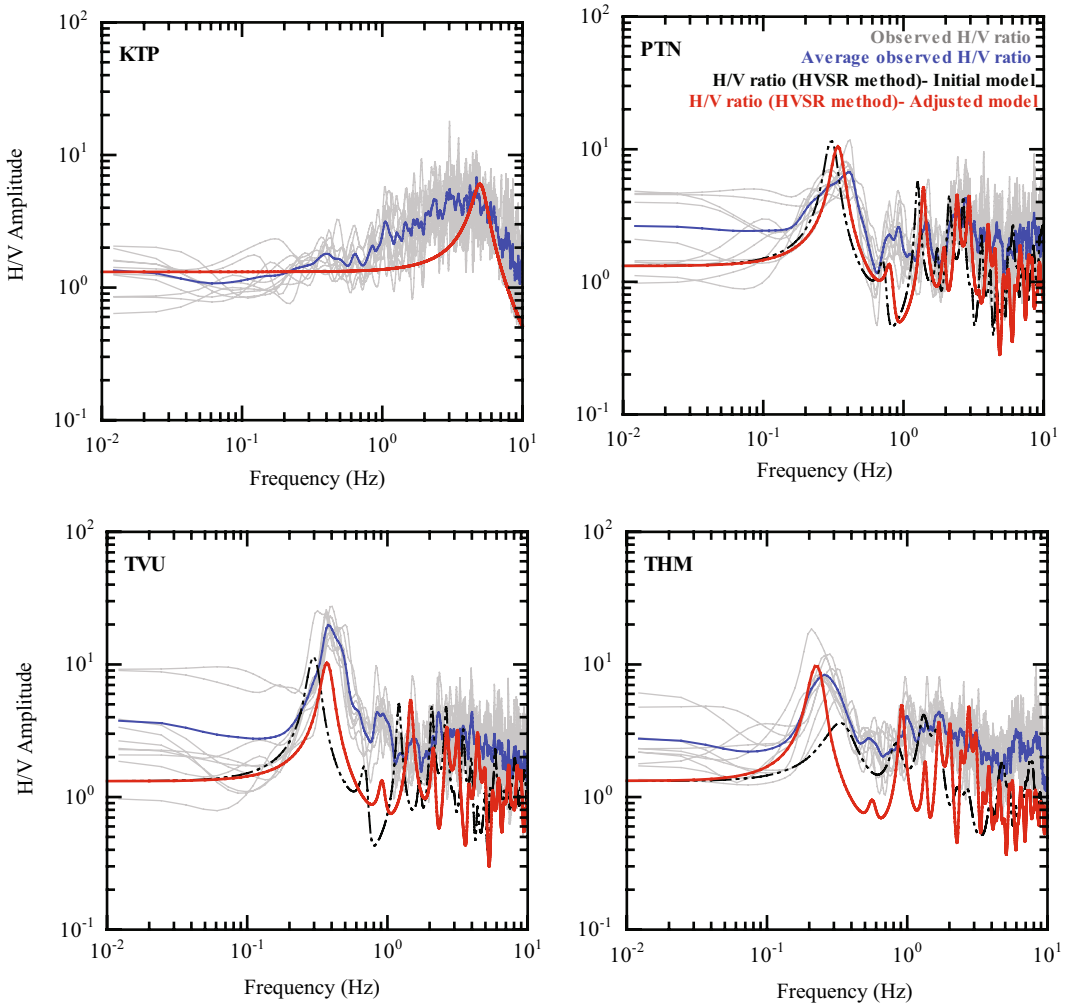

Fig. 12 Comparison of the observed average *H/V* ratio with the theoretical *H/V* ratio. The theoretical *H/V* ratio was calculated using the HVSR method and adjusted 1-D velocity model. Notice the flat curve at the rock site, KTP (<1 Hz). The *dashed black lines* indicate the results from the initial velocity models

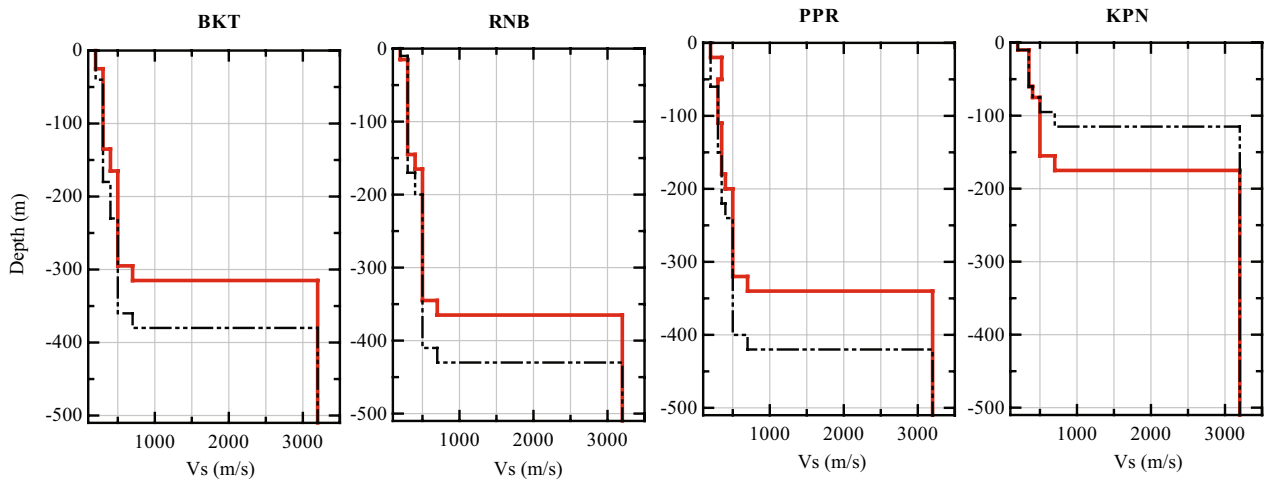

Fig. 13 1-D velocity models for the four temporary sites adjusted using the HVSR method. The site at KPN has the least sediment thickness, about 150 m. The *dashed black lines* show the initial velocity models for the four sites

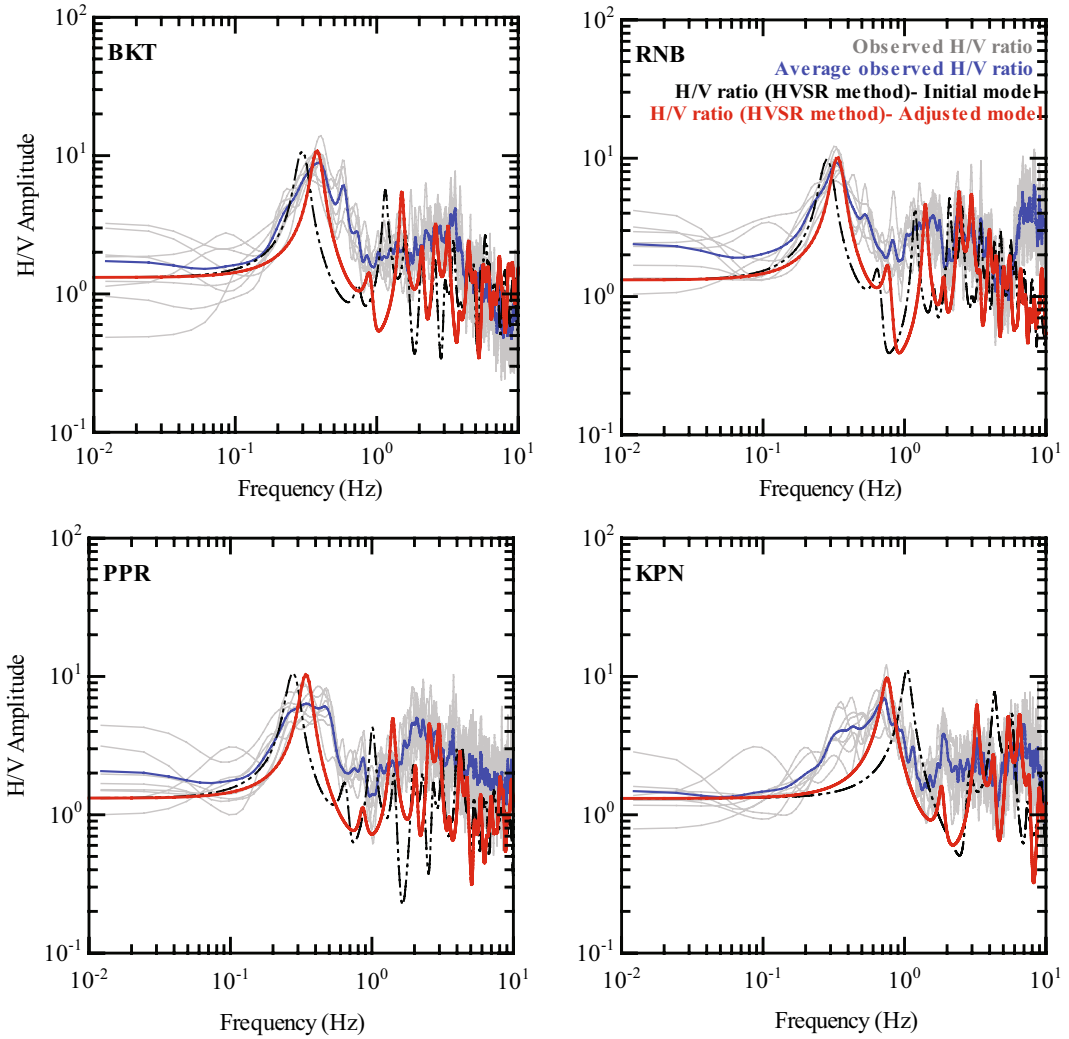

Fig. 14 Comparison of the observed and theoretical *H/V* ratios for the four temporary sites

using forward modeling of the observed long-period *S*-wave from mb4.9 deep earthquake. In this modeling, the observed long-period *S*-wave at the rock site was assumed as incident wave at the bedrock beneath the sedimentary sites. Third, the adjusted velocity models were verified by comparing the long-period simulated *S*-waves with the observed ones for three aftershocks (Mw5.1, Mw5.1, and Mw5.5) of the 2015 Gorkha Earthquake (Mw7.8). We have obtained fairly good agreement between the observed and simulated waveforms.

Finally, we examined the horizontal-to-vertical spectral ratios (*H*/*V* ratios) of earthquake ground motion to verify the adjusted velocity models estimated by forward modeling of the observed long-period *S*-wave. The observed *H*/*V* ratios agreed with the theoretical *H*/*V* ratios (Kawase et al. 2011) calculated from the adjusted velocity models in the low-frequency range; however, there were discrepancies between the observed and theoretical *H*/*V* ratios in the high-frequency range. We hypothesize that the HVSR method can also be used to estimate the subsurface geology in the Kathmandu Valley where the velocity contrast is high. The HVSR method is also a tool at our disposal to validate 1-D velocity models. The adjusted 1-D velocity models estimated by this study show the variation of sediment thickness beneath the sites. The bedrock depth varies from 155 to 440 m indicating an undulating basin topography of the Kathmandu Valley. The models show a high velocity contrast at the bedrock depth which results in significant *S*-wave amplification at the sediment sites. Our longer-term goal

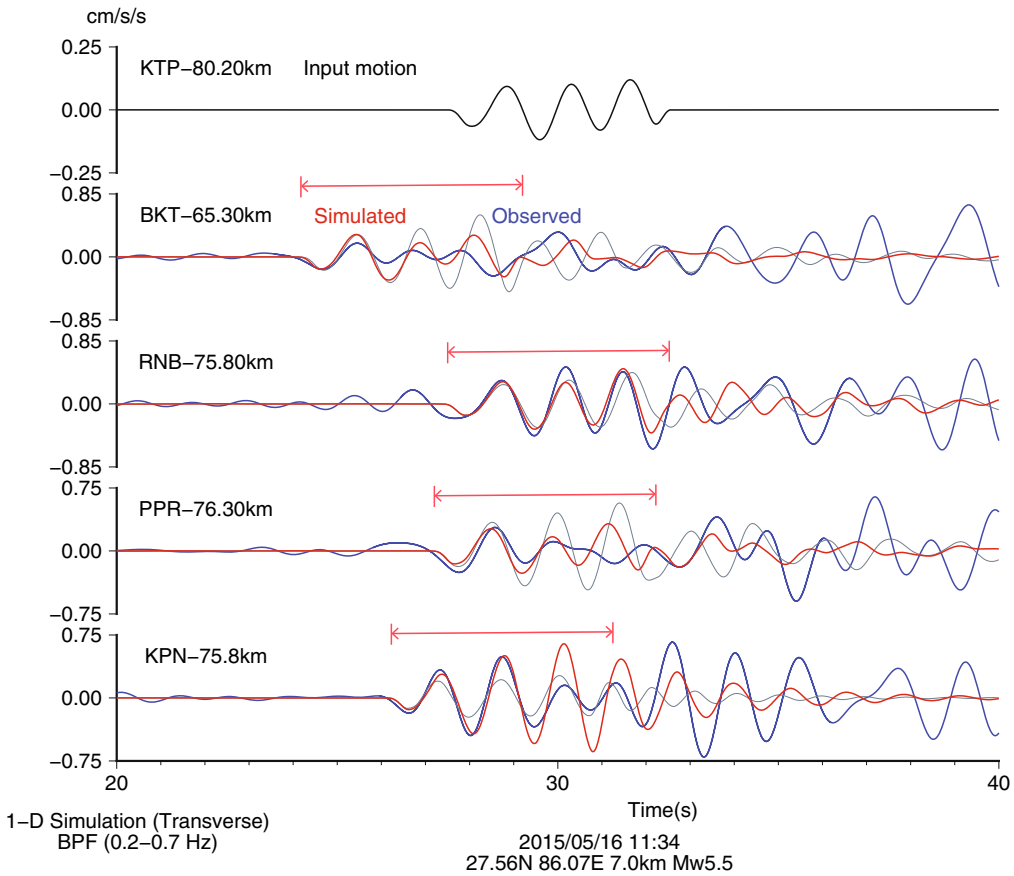

Fig. 15 Simulated and observed waveforms at the temporary sites for the Mw5.5 earthquake. Better agreement is provided in the results from the adjusted models (*red*) than from the initial model (*gray*). Waveform matching was conducted for time windows indicated by the *red arrows*

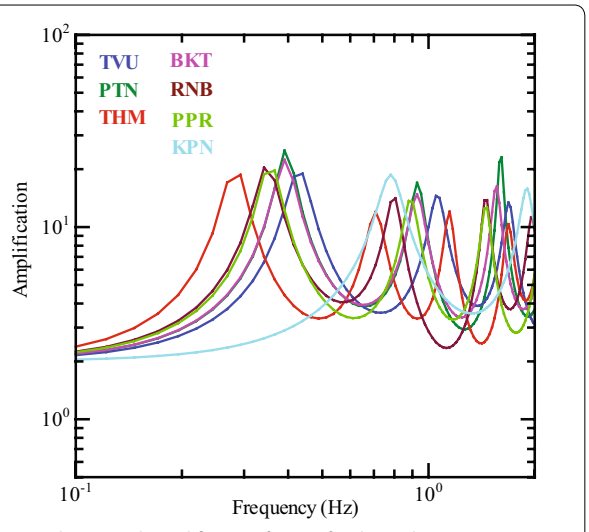

Fig. 16 Theoretical amplification factors for the sedimentary sites calculated using the Propagator Matrix method. There is a difference in fundamental peak between the sites, and significant amplification is clearly evident in the low-frequency range

is to prepare a full 3-D model of the subsurface geology of the valley using seismic waves, and this study is a first step in that task.

Authors' contributions

NT, TS, and MS designed the study. NT, MS, TS, MI, and SB aided in the installation and managing observations. YS collected the geological data and prepared the cross-sections. SB analyzed the data and drafted the manuscript. All authors read and approved the final manuscript.

Author details

[1] Graduate School of Engineering, Hokkaido University, Sapporo, Japan. [2] Faculty of Engineering, Hokkaido University, Sapporo, Japan. [3] Faculty of Human-Environment Studies, Kyushu University, Fukuoka, Japan. [4] Institute of Seismology and Volcanology, Hokkaido University, Sapporo, Japan. [5] Ainosato 1-4-19-12, Kita-ku, Sapporo, Japan. [6] Japan Water Agency, Saitama, Japan.

Acknowledgements

We acknowledge Prof. M.R. Dhital of Tribhuvan University, and Mr. S. Rajaure of Department of Mines and Geology, for help in installing and maintaining the instruments. Figure 1 is based on the Engineering Geological Map of Kathmandu printed by the Department of Mines and Geology (Shrestha et al. 1998). The Himalayan Main Frontal Thrust outline in Fig. 1 inset is based on Lave and Avouac (2000). We used GMT (Wessel et al. 2013) to prepare some of figures in the paper. The data for the location of the epicenters, depths, origin times, and magnitude were obtained from the United States Geological Survey (USGS 2015) portal. Part of this study was supported by the SATREPS

program of JST/JICA and J-RAPID program of JST and JSPS KAKENHI (Grant Numbers 16K06586, 16K16370, and 17H06215). We are grateful to two anonymous reviewers who gave their time to thoroughly review the manuscript and helped improve it.

Competing interests
The authors declare that they have no competing interests.

Publisher's Note

Received: 27 February 2017 Accepted: 14 July 2017
Published online: 24 July 2017

References

Aki K, Richards PG (2000) Quantitative seismology, 2nd edn. University Science Books, California

Bijukchhen S, Takai N, Shigefuji M, Ichiyanagi M, Sasatani T, Rajaure S, Dhital MR (2015) A comparative study of strong ground motion records from 30 August 2013 south Tibet earthquake on the rock and soil sites of Kathmandu Valley. J Nepal Geol Soc 48(Special Issue):48

Borah K, Kanna N, Rai SS, Prakasam KS (2015) Sediment thickness beneath the Indo-Gangetic Plain and Siwalik Himalaya inferred from receiver function modelling. J Asian Earth Sci 99:41–56. doi:10.1016/j.jseaes.2014.12.010

Dangol GMS (1985) Geology of the Kathmandu fluvial lacustrine sediments in the light of new vertebrate fossils occurrences. J Nepal Geol Soc 3:43–57

Dhakal YP, Sasatani T, Takai N (2009) Tuning the deep velocity structure model by 1-D simulation of long-period S-waves. In: Paper presented at the 9 SEGJ international symposium, Sapporo, Japan, 12–14 October 2009

Dhakal YP, Sasatani T, Takai N (2011) Validation of the deep velocity structure of the Tokachi basin based on 3-D simulation of long-period ground motions. Pure Appl Geophys 168(10):1599–1620. doi:10.1007/s00024-010-0237-3

Dhakal YP, Kubo H, Suzuki W, Kunugi T, Aoi S, Fujiwara H (2016) Analysis of strong ground motions and site effects at Kantipath, Kathmandu, from 2015 Mw7.8 Gorkha, Nepal, earthquake and its aftershocks. Earth Planets Space. doi:10.1186/s40623-016-0432-2

Dixit AM, Yatabe R, Dahal RK, Bhandary NP (2013) Initiatives for earthquake disaster risk management in the Kathmandu Valley. Nat Hazards 69(1):631–654. doi:10.1007/s11069-013-0732-9

Fujii R, Sakai H (2002) Paleoclimatic changes during the last 2.5 myr recorded in the Kathmandu Basin, Central Nepal Himalayas. J Asian Earth Sci 20:255–256

Government of Nepal (2015) Nepal disaster risk reduction portal. Government of Nepal. http://drrportal.gov.np/. Accessed 29 May 2017

Ichiyanagi M, Takai N, Shigefuji M, Bijukchhen S, Sasatani T, Rajaure S, Dhital MR, Takahashi H (2016) Aftershock activity of the 2015 Gorkha, Nepal, earthquake determined using the Kathmandu strong motion seismographic array. Earth Planets Space. doi:10.1186/s40623-016-0402-8

Japan International Cooperation Agency-JICA (2002) The study of earthquake disaster mitigation in the Kathmandu Valley, Kingdom of Nepal, vol I, II, and III. Japan International Cooperation Agency (JICA) and Ministry of Home Affairs Nepal, Kathmandu

Kawase H, Sanchez-Sesma FJ, Matsushima S (2011) The optimal use of horizontal-to-vertical spectral ratios of earthquake motions for velocity inversions based on diffuse-field theory for plane waves. Bull Seismol Soc Am 101(5):2001–2014. doi:10.1785/0120100263

Lave J, Avouac JP (2000) Active folding of fluvial terraces across the Siwaliks Hills, Himalayas of central Nepal. J Geophys Res Solid Earth 105(B3):5735–5770. doi:10.1029/1999jb900292

Monsalve G, Sheehan A, Schulte-Pelkum V, Rajaure S, Pandey MR, Wu F (2006) Seismicity and one-dimensional velocity structure of the Himalayan collision zone: earthquakes in the crust and upper mantle. J Geophys Res. doi:10.1029/2005jb004062

Moribayashi S, Maruo Y (1980) Basement topography of the Kathmandu Valley, Nepal: an application of gravitational method of the survey of a tectonic basin in the Himalayas. J Jpn Soc Eng Geol 21(2):30–37

Nagashima F, Matsushima S, Kawase H, Sanchez-Sesma FJ, Hayakawa T, Satoh T, Oshima M (2014) Application of horizontal-to-vertical spectral ratios of earthquake ground motions to identify subsurface structures at and around the K-NET site in Tohoku, Japan. Bull Seismol Soc Am 104(5):2288–2302. doi:10.1785/0120130219

Olsen KB, Nigbor R, Konno T (2000) 3D viscoelastic wave propagation in the Upper Borrego Valley, California, constrained by borehole and surface data. Bull Seismol Soc Am 90(1):134–150

Pandey MR (2000) Ground response of Kathmandu Valley on the basis of microtremors. In: Paper presented at the 12th world conference on earthquake engineering, Auckland, New Zealand, 30 January–4 February 2000

Paudyal YR, Yatabe R, Bhandary NP, Dahal RK (2012) A study of local amplification effect of soil layers on ground motion in the Kathmandu Valley using microtremor analysis. Earthq Eng Eng Vib 11(2):257–268. doi:10.1007/s11803-012-0115-3

Paudyal YR, Yatabe R, Bhandary NP, Dahal RK (2013) Basement topography of the Kathmandu Basin using microtremor observation. J Asian Earth Sci 62:627–637. doi:10.1016/j.jseaes.2012.11.011

Piya BK (2004) Generation of a geological database for the liquefaction hazard assessment in Kathmandu Valley. MSc Thesis, International Institute for Geo-Information and Earth Observation (ITC), The Netherlands

Rajaure S, Asimaki D, Thompson EM, Hough S, Martin S, Ampuero JP, Dhital MR, Inbal A, Takai N, Shigefuji M, Bijukchhen S, Ichiyanagi M, Sasatani T, Paudel L (2016) Characterizing the Kathmandu Valley sediment response through strong motion recordings of the 2015 Gorkha earthquake sequence. Tectonophysics. doi:10.1016/j.tecto.2016.09.030

Sakai H (2001) Stratigraphic division and sedimentary facies of the Kathmandu Basin Group, central Nepal. J Nepal Geol Soc 25(Sp. Issue):19–32

Sakai H, Fujii R, Kuwahara Y, Upreti BN, Shrestha SD (2001) Core drilling of the basin-fill sediments in the Kathmandu Valley for palaeoclimatic study: preliminary results. J Nepal Geol Soc 25(Special Issue):9–18

Sakai H, Fujii R, Kuwahara Y (2002) Changes in the depositional system of the Paleo-Kathmandu Lake caused by uplift of the Nepal Lesser Himalayas. J Asian Earth Sci 20(3):267–276. doi:10.1016/S1367-9120(01)00046-3

Sapkota SN, Bollinger L, Klinger Y, Tapponnier P, Gaudemer Y, Tiwari D (2013) Primary surface ruptures of the great Himalayan earthquakes in 1934 and 1255. Nat Geosci 6(1):71–76

Satoh T (2004) Inversion of incident angle and Q value of sediments from deep borehole seismograms using adaptive simulated annealing method. In: Paper presented at the 13 world conference on earthquake engineering, Vancouver, Canada, 1–6 August 2004

Shrestha OM, Koirala A, Karmacharya SL, Pradhananga UB, Pradhan P, Karmacharya R (1998) Engineering and environmental geological map of the Kathmandu Valley. Department of Mines and Geology, Kathmandu

Stocklin J, Bhattarai KD (1977) Geology of Kathmandu area and central Mahabharat range, Nepal himalaya. HMG/UNDP Mineral Exploration Project, Kathmandu

Takai N, Sawada K, Shigefuji M, Bijukchhen SM, Ichiyanagi M, Sasatani T, Dhakal YP, Rajaure S, Dhital MR (2015) Shallow underground structure of strong ground motion observation sites in the Kathmandu Valley. J Nepal Geol Soc 48(Special Issue):50

Takai N, Shigefuji M, Rajaure S, Bijukchhen SM, Ichiyanagi M, Dhital MR, Sasatani T (2016) Strong ground motion in the Kathmandu Valley during the 2015 Gorkha, Nepal, Earthquake. Earth Planets Space. doi:10.1186/s40623-016-0383-7

United States Geological Survey-USGS (2015) Earthquake hazards program. http://earthquake.usgs.gov/. Accessed 3 March 2017

Wessel P, Smith WHF, Scharroo R, Luis J, Wobbe F (2013) Generic mapping tools: improved version released. EOS Trans Am Geophys Union 94:409–410. doi:10.1002/2013EO450001

Yoshida M, Igarashi Y (1984) Neogene to quaternary lacustrine sediments in the Kathmandu Valley, Nepal. J Nepal Geol Soc 4(Special Issue):73–100